The following publication J. Pan, J. Zhou, X. Yi, Q. Sui, C. Lu and Z. Li, "Multi-Dimensional Optical Fiber Sensing Enabled by Digital Coherent Optical Technologies," in Journal of Lightwave Technology, vol. 37, no. 11, pp. 2488-2501, 1 June, 2019 is available at https://doi.org/10.1109/JLT.2018.2865747.

Multi-Dimensional Optical Fiber Sensing Enabled by Digital Coherent Optical Technologies

Jingshun Pan, Ji Zhou, Xingwen Yi, Chao Lu, and Zhaohui Li

***Abstract*—Optical fiber sensing (OFS) systems can be used to accurately measure temperature, strain, pressure and other physical parameters by detecting the change in the field of lightwave. As they are used in more application areas, a new type of OFS with the ability of providing multi-dimensional, highly sensitive, ultra-fine and real-time measurement is necessary. This is possible with the application of digital coherent optical technologies in the OFS systems. In this paper, we show that many aspects of OFS systems can be replaced or enhanced by digital coherent optical technologies. For example, digital optical frequency comb (DOFC) can replace the sweeping laser source, and the digital coherent optical receiver can replace direct detection receiver to enable simultaneously detect all the dimensions of lightwave. Based on these techniques, we present our research progresses on OFS with multi-dimensional, real-time, ultra-fine spectral analysis, and single-shot Brillouin optical time-domain analysis based DOFC for distributed OFS. We show that the OFS systems can be bought to a whole new level with the capabilities of real-time time-frequency analysis, ultra-fine spectral resolution and ultra-low sensitivity. Opportunities and challenges of using digital coherent optical technologies in OFS systems are also discussed.**

***Index Terms*—Digital Coherent Optical Technology, Digital Optical Frequency Comb, Brillouin optical time-domain analysis, Optical fiber sensing**

I. Introduction

IN RECENT YEARS, optical fiber sensing (OFS) has been widely applied in various military, industry, and biomedical fields, to accurately measure strain, temperature, pressure and other parameters [1-3]. Unlike conventional electrical and electronic sensors, OFS can accomplish reliable sensing tasks in challenging environment with the presence of high voltage and flammable material, such as in aircraft jet engines, aerospace and electrical switchgear [4]. When it is applied to various new fields, new challenges arise [5, 6]. Many of the new applications such as typhoon warning, earthquake detection and cosmic phenomenon monitoring require multi-dimensional sensing, highly sensitive, ultra-fine and real-time signal measurement. As a result, new type of OFS needs to be developed.

In terms of signal processing techniques employed at the transmitter and receiver. OFS and optical fiber transmissions share many similarities. Although it is simplified, we may use a simple structure in Fig. 1 (a) for both of them. A main difference is that for optical transmission, the transmitter and receiver are typically at different physical locations while for OFS they are typically at the same location. In the early days, OFS and optical fiber transmissions had to compete with their mature electronic counterparts. Therefore, the transmitter and receiver of OFS need to be as simple as possible. As a result, the signal processing employed was analog and one-dimensional, as shown in Fig. 1 (b).

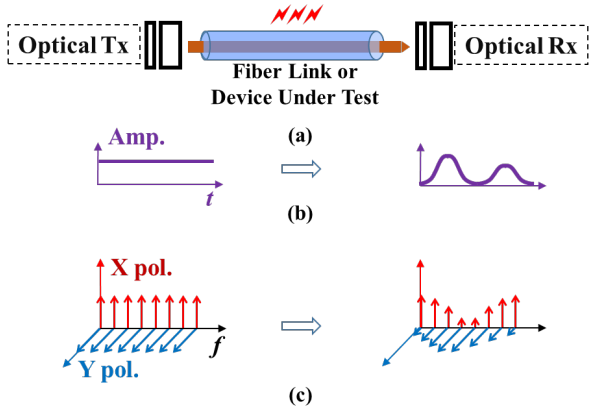

Fig. 1. (a) Simplified concept diagram for optical fiber sensing and transmission. (b) One-dimensional and analog scenario. (c) Multi-dimensional and digital scenario.

The drawbacks of analog signal processing are well understood from the transition from analogue to digital signal processing (DSP) in optical fiber transmissions. i) The analog signal processing tends to offer simpler functions, which cannot deal with the complicated distortion effectively, whereas DSP can be quite sophisticated based on memory and logic operations. ii) The analog signal processing may require high-precision devices, which is problematic at some extreme

This work was supported in part by Local Innovative and Research Teams Project of Guangdong Pearl River Talents Program 2017BT01X12. Corresponding author: Ji Zhou, Xingwen Yi, Zhaohui Li.

Jingshun Pan, Xingwen Yi, Zhaohui Li is with State Key Laboratory of Optoelectronic Materials and Technologies and School of Electronics and Information Technology, Sun Yat-sen University, Guangzhou, 510275, China. Email: yixw5@mail.sysu.edu.cn, lzhh88@mail.sysu.edu.cn.

Ji Zhou is with Department of Electronic Engineering, College of Information Science and Technology, Jinan University, Guangzhou 510632, China. Email: zhouji_jnu@163.com.

Chao Lu is with the Department of Electronic and Information Engineering, The Hong Kong Polytechnic University, Hong Kong.

conditions. iii) The impact of noise on analog system performance is more significant and can not be easily removed.

One-dimensional OFS is simple, but with limited capabilities. i) In nature, not many phenomena happen individually and not many effects only induce one-dimensional variation. Therefore, some effects are coupled together and in fact, the decoupling is crucial in many OFS. The ability to detect multi-dimensional signal can certainly facilitate the decoupling. ii) As we know, from optical fiber transmission, the one-dimensional measurement of amplitude has a limited sensitivity of detection, which limits its applications in the remote sensing. iii) In the scenario of multi-parameter monitoring, the use of one-dimensional measurement may be bulky and expensive.

Recently, digital coherent optical technology has been employed to communicate, store, and process multi-dimensional information in a growing number of applications [7], such as optical fiber transmission [8], OFS [9], gated holographic imaging [10], and three dimensional optical data storage [11]. In optical fiber transmissions, if not digital everything, many pivotal signal processing functions have become digital. The first notable transition from analog to digital is digital phase estimation that estimates and compensates the laser phase noise in the digital domain. Therefore, the lasers at the transmitter and receiver only need an approximate frequency alignment but not phase-locked. Digital phase estimation removes the need for optical phase locked loop which often can only work well in a laboratory environment, and heralded the era of the digital coherent optical technology. Digital dispersion compensation has circumvented the optical dispersion compensation module that is not only expensive but also insufficient for dynamic and accurate dispersion compensation, indispensable requirements from high baud-rate and long-distance fiber transmission. Digital polarization de-multiplexing has totally eliminated the optical polarization tracking module for high spectrum efficiency transmission. Without further listing the other digital signal processing functions, we have already witnessed the success of digital coherent optical technology, which has enabled the unprecedented high-capacity, long-distance transmissions exploiting various advanced modulation formats [12], such as phase-shift keying (PSK), quadrature-amplitude modulation (QAM) and orthogonal frequency-division multiplexing (OFDM) [13-15].

Although there were many concerns of the cost of digital coherent optical technology a few years ago, they are gradually dismissed by the advances of silicon technology. In fact, its cost will be lowered further with the successful mass production. Owing to advances in silicon technology, the CMOS analog-to-digital converter (ADC) can achieve the sample rate of higher than 100 GS/s, which makes high-speed DSP available for the high-capacity optic fiber transmission. Recently, 100-Gb/s coherent optic fiber transmission has been widely deployed in commercial optical networks [16]. Higher baud-rate transmission of 120 GBaud [17] and higher-capacity transmission of 71.65 Tbit/s [18] have been demonstrated to meet the demands of the future optical networks. With the development in optical fiber communications, the cost of digital coherent optical technology is always on a downward track. Therefore, the multi-dimensional information can be effectively handled by low-cost digital coherent optical technology, which can promote the advance of other cost-sensitive optical information systems, such as optical fiber sensing.

Similar evolution is taking place in optical fiber sensing. Fig. 1(c) shows an example of multi-dimensional OFS heavily relying on digital signal processing. In addition to digital coherent optical receiver, digital optical frequency comb (DOFC) has been proposed and applied in spectrum analysis in optical fiber sensing. Conventional methods replying on laser scanning and mechanical tuning of grating in the optical spectrum analyzer (OSA) have the drawbacks of low resolution, low measurement speed and no phase response. The spectral analysis based on optical frequency comb is widely used in accurate frequency measurement, atomic and molecular spectroscopic analysis. However, the optical frequency comb is usually generated by optical method and thus with large comb spacing, which limits the resolution of spectral analysis. Recently, ultra-fine spectral analysis technology based on digital optical frequency comb (DOFC) combined with digital coherent optical receiver has received great attention [19-22] with the advantages of

- ✓ Fast and real time (no averaging) capturing ability.
- ✓ High sensitivity/accuracy.
- ✓ High resolution.
- ✓ High throughput sampling ability.
- ✓ Multi-dimensional information detecting ability.

This paper will focus on the principle of ultra-fine spectral analysis technology and its applications in OFS. The main contributions of this paper are as follows:

- OFS based on ultra-fine spectral analysis: The principle of ultra-fine spectral analysis based on DOFC, OFS based on ultra-fine spectral analysis, and optical spectrum stitching for ultra-wide spectral analysis are introduced. The feasibility and advantages of ultra-fine spectral analysis based on DOFC are experimentally demonstrated.
- Brillouin optical time-domain analysis (BOTDA) based on DOFC for distributed OFS: Our progresses on the BOTDA based on DOFC for distributed OFS are introduced in detail, including scanning-free BOTDA based on DOFC, single-shot BOTDA based on DOFC and coherent detection, and spatial resolution improvement of single-shot DOFC-based BOTDA utilizing multiple pump pulses.

The rest of the paper are as follows. In Section II, the coherent optical receiver, DOFC and distortion compensation are introduced. In Section III, the OFS based on ultra-fine spectral analysis is demonstrated. In Section IV, BOTDA based on DOFC for distributed OFS is introduced. The article concludes in Section V.

II. Coherent Optical Receiver and DOFC Technology

Coherent optical receiver is used to simultaneously detect all the dimensions of a lightwave signal. We briefly describe a

coherent optical receiver and then discuss the related digital coherent signal processing techniques.

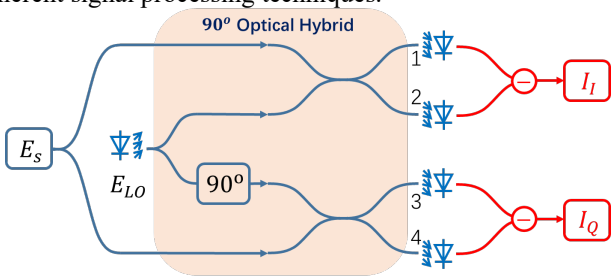

Fig. 2. Coherent optical receiver based on 90^o optical hybrid and balanced photodiode.

A. Coherent Optical Receiver

Figure 2 depicts coherent optical receiver based on 90° optical hybrid, local oscillator (LO) and balanced photodiode (BPD). The 90° optical hybrid mainly consists of two 3-dB optical couplers and 90° phase shifter. For simplicity, we describe the ideal condition first and then will discuss the use of digital coherent optical technology to compensate for the non-ideal conditions of the components. The outputs of two 3-dB optical couplers can be expressed as

$$E_1 = \frac{1}{\sqrt{2}}\left(E_S + E_{LO}\right), \quad E_2 = \frac{1}{\sqrt{2}}\left(E_S - E_{LO}\right)$$
$$E_3 = \frac{1}{\sqrt{2}}\left(E_S - jE_{LO}\right), \quad E_4 = \frac{1}{\sqrt{2}}\left(E_S + jE_{LO}\right) \tag{1}$$

After O/E conversion, the detected electrical signals are

$$I_1 = R\times|E_1|^2 = \frac{R}{2}\left[|E_S|^2 + |E_{LO}|^2 + 2\,\mathrm{Re}\left(E_S E_{LO}^*\right)\right]$$
$$I_2 = R\times|E_2|^2 = \frac{R}{2}\left[|E_S|^2 + |E_{LO}|^2 - 2\,\mathrm{Re}\left(E_S E_{LO}^*\right)\right]$$
$$I_3 = R\times|E_3|^2 = \frac{R}{2}\left[|E_S|^2 + |E_{LO}|^2 + 2\,\mathrm{Im}\left(E_S E_{LO}^*\right)\right] \tag{2}$$
$$I_4 = R\times|E_4|^2 = \frac{R}{2}\left[|E_S|^2 + |E_{LO}|^2 - 2\,\mathrm{Im}\left(E_S E_{LO}^*\right)\right]$$

After the balanced detection, the electrical signals of in-phase and quadrature paths can be obtained from

$$I_I = I_1 - I_2 = 2R\times\mathrm{Re}\left(E_S E_{LO}^*\right)$$
$$I_Q = I_3 - I_4 = 2R\times\mathrm{Im}\left(E_S E_{LO}^*\right) \tag{3}$$

Finally, the signal is recovered by combining the I_I with I_Q

$$I = I_I + jI_Q = 2R\times E_S E_{LO}^* \tag{4}$$

Equation 4 shows that the coherent optical receiver can convert optical signal to electrical signal with amplitude and phase information. Further extension of Fig. 2 by polarization diversity technique is straightforward and then all the dimensions of optical signal are recovered [23]. Eq. 4 also explains the superior sensitivity of coherent optical receiver where the local oscillator can provide a gain to the signal and consequently, the quantum noise limited sensitivity can be achieved.

B. Ultra-Fine Spectral Analysis Based on DOFC

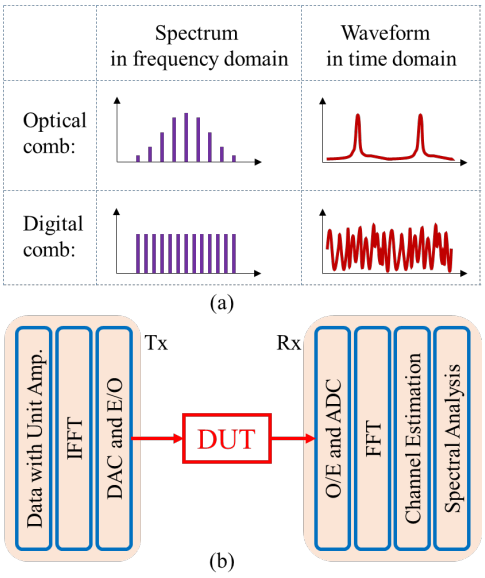

Fig. 3. (a) Comparison of optical comb and digital comb. (b) Principle of ultra-fine spectral analysis based on DOFC.

As per the discussion aforementioned, spectral analysis using scanning frequency source can be replaced by DOFC, which generates digital frequency comb (DFC) first, and then uploads DFC into digital-to-analog converter (DAC) for producing DEFC, and finally converts it to optical domain. DFC is greatly inspired by OFDM which carries data in multiple orthogonal subcarriers [24-26]. As shown in Fig. 3(a), the envelop of the spectrum of optical comb is generally Gaussian, and the time domain waveform consists of periodic pulses. These features are not desirable when we use optical comb to replace the sweeping frequency sources for ultra-fine spectrum analysis. Instead, we find digital comb with a capability to well control the spectrum envelop can serve our purpose perfectly. As shown in Fig. 3(b), the brick-wall shaped envelop means that it can provide uniform frequency lines at different frequencies. The irregular time-domain waveform is also better than the pulsed one of optical comb, which can be challenging for electrical and optical components.

In general, multiple frequency lines can be expressed as

$$\xi_{\mathrm{DEFC}}\left(f\right) = \sum_{q=0}^{N-1} E_q \exp\left(j\varphi_q\right)\cdot\delta\left(f - f_q\right) \tag{5}$$

where E_q, φ_q and f_q are amplitude, phase and frequency of the q-th comb line, respectively; $f_q = q\Delta f$, Δf is the constant minimum comb spacing, and N is the total number of comb lines.

The corresponding time-domain optical waveform of DEFC can be defined as

$$E_{DEFC}\left(t\right) = \frac{1}{2\pi}\sum_{q=0}^{N-1} E_q \exp\left(j2\pi q\Delta ft + j\varphi_q\right) \tag{6}$$

If the time duration of the waveform in Eq. 6 is T_s, the so-called orthogonal condition is

$$T_s\times\Delta f = 1 \tag{7}$$

then the multiple frequency lines are the well-studied

orthogonal subcarriers in OFDM [24-26]. Consequently, the time-domain waveform in Eq. 6 can be readily computed from Eq. 5 by the efficient digital algorithm of fast Fourier transform (FFT),

$$\begin{aligned}\xi_{\mathrm{DEFC}}(f)&=\mathrm{FFT}\left[E_{DEFC}(t)\right]\\&=\frac{1}{2\pi}\sum_{q=0}^{N-1}E_q\exp\left(j\varphi_q\right)\cdot\mathrm{FFT}\left[\exp\left(j2\pi q\Delta ft\right)\right]\\&=\sum_{q=0}^{N-1}E_q\exp\left(j\varphi_q\right)\delta\left(f-q\Delta f\right)\\&=\sum_{q=0}^{N-1}E_q\exp\left(j\varphi_q\right)\delta\left(f-f_q\right)\end{aligned}\tag{8}$$

The so-generated multiple frequency lines form a digital frequency comb (DFC). It is now clear that the advantage of using digital signal processing of FFT is that we can design the frequency comb directly in the frequency domain by setting proper parameters and then convert it to the time domain for signal generation. There are three immediate features. i) We can generate a comb source with the brick-wall shaped envelop, which is difficult for the optical comb, as shown in Fig. 3(a). ii) The frequency spacing of the comb can be readily changed, which again is challenging for the optical comb. iii) Note that when we use the comb to replace the sweeping frequency source, there is no requirement on the phase. As shown in Fig. 3(a), we can use this extra freedom to control the time-domain waveform, such as to avoid the pulsed one. This freedom is certainly not available from the optical comb.

Once we have DFC, we can up-convert it to optical domain, co-called DOFC, and use it for spectrum measurement. Fig. 3(b) shows the principle of ultra-fine spectral analysis starting from DFC. Here, we focus on the principle and certainly many more procedures can be included according to different applications. At the transmitter, the IFFT is employed to multiplex the input data to generate the DFC. DFC is uploaded into digital-to-analog converter (DAC) for producing DEFC. E/O modulator modulates the optical source with DEFC to generate DOFC. The generated DOFC is fed into the DUT. At the receiver, the DOFC after the DUT is processed by the inverse operation of the transmitter. After FFT, the channel estimation is used to measure the frequency-domain information of the DOFC to implement the spectral analysis for DUT.

After the DUT, the received frequency-domain DOFC can be described as

$$R_{\mathrm{DOFC}}(f)=\sum_{q=0}^{N-1}E_q\exp\left(j\varphi_q\right)\cdot\delta\left(f-f_q\right)H(f_q)\tag{9}$$

where $H\left(f_q\right)$ is a frequency-dependent complex transfer function, which expresses the channel response of DUT,

$$H\left(f_q\right)=G\left(f_q\right)\exp\left[j\phi\left(f_q\right)\right]\tag{10}$$

At the receiver, an inverse process can be applied to estimate the channel response of DUT, $H\left(f_q\right)$, including O/E conversion, ADC, FFT, channel estimation. The channel estimation can be implemented by

$$H\left(f_q\right)=R_{\mathrm{DOFC}}\left(f_q\right)/T_{\mathrm{DOFC}}\left(f_q\right)\tag{11}$$

where T_{DOFC} is the frequency-domain transmitted DOFC. The estimated $H\left(f_q\right)$ can be used to implement the ultra-fine spectral analysis.

C. Distortion Compensation for DOFC

So far, we describe the DOFC system with ideal components. For practical applications, the powerful digital coherent optical technology can be used to compensate for various imperfect conditions. As examples, we explain the distortion compensation for IQ imbalance, polarization rotation, and phase noise.

1. IQ imbalance compensation

At the receiver, there is IQ imbalance in the 90° optical hybrid. Therefore, I and Q components are no longer orthogonal. The Gram-Schmidt algorithm can create a set of mutually orthogonal vectors, which can be employed to compensate the non-orthogonality between I and Q components [27]. The output vector of Gram-Schmidt algorithm can be expressed as

$$\begin{bmatrix}\mathrm{OUT}_I\\ \mathrm{OUT}_Q\end{bmatrix}=\begin{bmatrix}1 & 0\\ -\dfrac{\langle R_IR_Q\rangle}{\langle R_I^2\rangle} & 1\end{bmatrix}\begin{bmatrix}R_I\\ R_Q\end{bmatrix}\tag{12}$$

where R_I and R_Q are the received I and Q components, respectively. Obviously, the output vector of Gram-Schmidt algorithm is orthogonal. Therefore, the Gram-Schmidt algorithm can compensate the non-orthogonality of imperfect 90° optical hybrid.

2. Digital polarization rotation

In an optical fiber, the polarization rotation can be described by Jones matrix, and now, tracking the polarization is done by digital polarization rotation. We may need some time-multiplexed training symbols on X and Y polarizations, as shown in Fig. 4 [28]. The frequency-domain training symbols can be expressed as

$$T_X=\begin{bmatrix}T_{X,t1}\\ 0\end{bmatrix},\quad T_Y=\begin{bmatrix}0\\ T_{Y,t2}\end{bmatrix}\tag{13}$$

where T_X and T_Y are the training symbols on X and Y polarizations, respectively. The received training symbols can be defined as

$$\begin{bmatrix}R_{X,t1}\\ R_{Y,t1}\end{bmatrix}=\begin{bmatrix}H_{XX} & H_{XY}\\ H_{YX} & H_{YY}\end{bmatrix}\begin{bmatrix}T_{X,t1}\\ 0\end{bmatrix}=\begin{bmatrix}H_{XX}T_{X,t1}\\ H_{YX}T_{X,t1}\end{bmatrix}\tag{14}$$

$$\begin{bmatrix}R_{X,t2}\\ R_{Y,t2}\end{bmatrix}=\begin{bmatrix}H_{XX} & H_{XY}\\ H_{YX} & H_{YY}\end{bmatrix}\begin{bmatrix}0\\ T_{Y,t2}\end{bmatrix}=\begin{bmatrix}H_{XY}T_{Y,t2}\\ H_{YY}T_{Y,t2}\end{bmatrix}\tag{15}$$

Since the training symbols are known, the Jones matrix can be obtained from

$$H=\begin{bmatrix}H_{XX} & H_{XY}\\ H_{YX} & H_{YY}\end{bmatrix}=\begin{bmatrix}R_{X,t1}/T_{X,t1} & R_{X,t2}/T_{Y,t2}\\ R_{Y,t1}/T_{X,t1} & R_{Y,t2}/T_{Y,t2}\end{bmatrix}\tag{16}$$

Once we have the Jones matrix H, we may start to track the polarization of any received signal by simply dividing H, or multiplexing the inverse of H,

$$\begin{bmatrix} \mathrm{DATA}_X \\ \mathrm{DATA}_Y \end{bmatrix} = \begin{bmatrix} H_{XX} & H_{XY} \\ H_{YX} & H_{YY} \end{bmatrix}^{-1} \begin{bmatrix} \mathrm{Probe}\ X \\ \mathrm{Probe}\ Y \end{bmatrix} \quad (17)$$

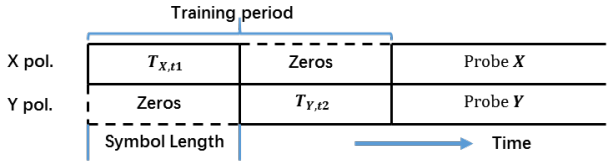

Fig. 4. Time-multiplexed training symbols for digital polarization rotation.

3. *Digital phase compensation*

The implementation of digital phase compensation may vary slightly in different systems. In DOFC, the pilot signals are inserted in the subcarriers of DOFC signal to estimate the phase noise [29, 30]. The estimated phase noise can be defined as

$$\phi = \frac{1}{N_p}\sum_{k=1}^{N_p}\left[\arg\left(Y_k\right) - \arg\left(X_k\right)\right] \quad (18)$$

where X_k is the pilot signal on the subcarrier of DOFC and Y_k is the received pilot signal. The estimated phase noise can be employed to implement the phase recovery in the DOFC system.

In conclusion, after the distortion compensation, the coherent DOFC technology can be employed to simultaneously recover the multi-dimensional information from the received signal, including polarization, amplitude, phase and frequency. Therefore, the coherent DOFC technology have the potential for multi-dimensional detection and analysis in the OFS.

III. OFS Based on Ultra-Fine Spectral Analysis

In this section, the principle of ultra-fine spectral analysis based on DOFC, OFS based on ultra-fine spectral analysis, and optical spectrum stitching for ultra-wide spectral analysis are introduced. The feasibility and advantages of ultra-fine spectral analysis based on DOFC are experimentally demonstrated.

A. Ultra-fine Spectral Analysis Based on DOFC

We set up an experimental system to demonstrate the feasibility of the ultra-fine spectral analysis based on DOFC. The brief experimental setup is shown as Fig. 3. The DUT is a home-built delay interferometer with 8-meter length mismatch, which is very unstable due to the uncontrolled interferometric structure. Therefore, the DUT cannot be characterized by other methods with slow measurement speed, e.g., optical spectrum analyzer. In our measurement, we can realize real-time time-frequency analysis since the digital coherent optical receiver and DOFC can acquire real-time information of the DUT. Fig. 5 shows the real-time spectrogram of both amplitude and phase. The frequency and phase responses can be instantly measured at a speed of 1.45 μs. The stationary amplitude and phase responses simply mean that our measurement speed is much faster than the variation speed of the delay interferometer. We may record a dynamic amplitude and phase responses if we increase the measure time window.

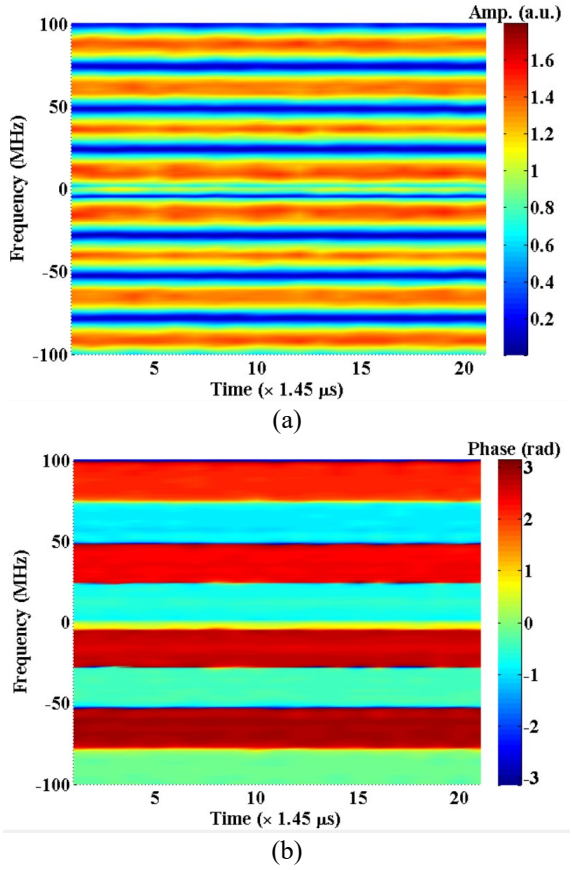

Fig. 5. Real-time spectrogram of both (a) amplitude and (b) phase information.

Figure 6 shows the spectrum and phase response of DUT measured by the ultra-fine spectral analysis. The free spectral range (FSR) is 25.4 MHz at a resolution of 0.732 MHz. If the refractive index of the optical fiber is 1.5, via the FSR, the length mismatch of the delay interferometer is calculated as 7.8686 meter with an accuracy of 0.22 meter. The proposed ultra-fine spectral analysis based DOFC can accurately measure the discrete phase level with a difference of π and the periodic phase jumps which can reflect the phase response of the delay interferometer. Meanwhile, the spectral resolution and other key parameters can be modified easily since they are controlled by the DSP.

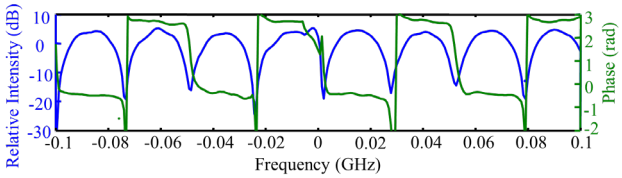

Fig. 6. Free spectral range (FSR) of the home-built delay interferometer [31].

B. Ultra-Fine Spectral Analysis for OFS

Next, fast and high-precision measurement for OFS is implemented by the ultra-fine spectral analysis based on DOFC. A Mach-Zehnder refractive index sensor is employed to demonstrate the feasibility of the ultra-fine spectral analysis.

Figure 7 shows the schematic diagram of OFS based on the ultra-fine spectral analysis. At the transmitter, a user-defined sequence based on Eq. (8) is subject to the IFFT for generating

the DFC. The DAC is employed to convert the DFC to the DEFC, which is then used to modulate the optical source to produce DOFC as shown in inset a of Fig. 7. After DUT, the amplitude, phase and/or polarization of DOFC are changed as shown in inset b. The digital coherent optical receiver can accurately detect these changes. Its electrical outputs are captured by ADC. The recovered digital signals are processed by offline DSP to measure the accurate spectrum, as shown in inset c of Fig. 7.

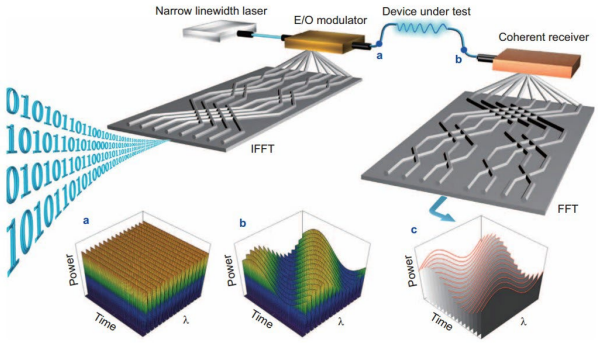

Fig. 7. Schematic diagram of OFS based on ultra-fine spectral analysis. Inset a: The generated DOFC. Inset b: The DOFC after DUT. Inset c: The recovered spectrum at the receiver [9].

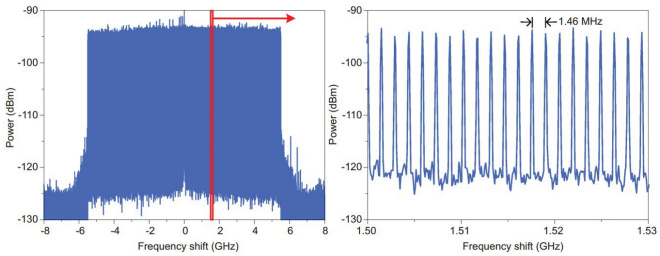

Fig. 8. Measured spectrum of DOFC before DUT with a minimum frequency spacing of 1.46 MHz [9].

The measured spectrum of the DOFC before DUT is depicted in Fig. 8. The sample rate of the DAC is set to 12 GS/s. For a good anti-noise ability and reliability, the high-frequency comb lines are set to the power of 0, which is from -6 to -5 GHz and +5 to +6 GHz. Therefore, the frequency range of the measured spectrum is from -5 to +5 GHz. As shown in zoom view of Fig. 8, the minimum frequency spacing of comb lines is approximately 12 GHz/8192 = 1.46 MHz, which is ~0.01 pm at the central wavelength of 1550 nm. By this way, a DOFC with a minimum frequency spacing of 1.46 MHz is generated in the range from -5 to 5 GHz.

In this experiment, ethanol is used as the sample liquid for measuring the relationship between refractive index and temperature by OSA (0.002-nm resolution) and ultra-fine spectral analysis based on DOFC. The measured transmission spectra of the MZI sensing unit are shown in Fig. 9. The phase of the MZI changes with the temperature. The measured transmission spectrum of the MZI moves to the higher frequency with the increase of phase. The period of the transmission spectrum is approximately 5.5 GHz, corresponding to the optical path difference of 0.055 m.

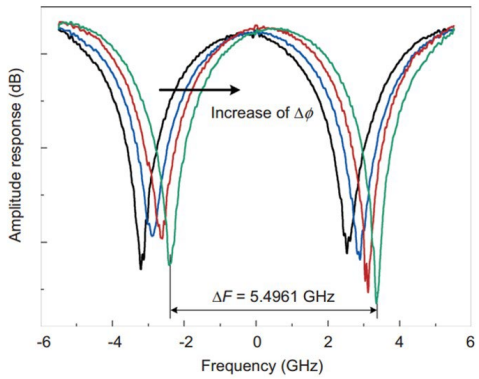

Fig. 9. Measured transmission spectrum of MZI sensing unit when ethanol is used as sample liquid [7].

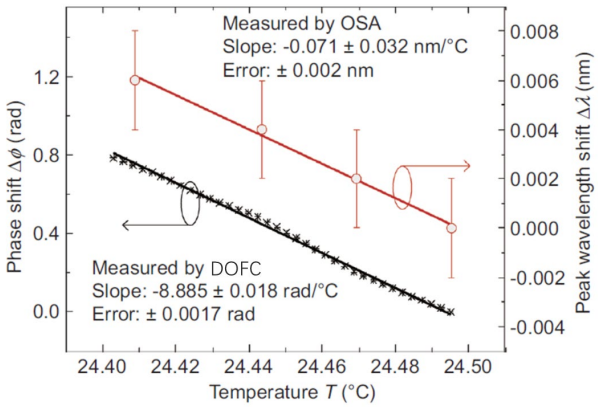

Fig. 10. Phase change measured by ultra-fine spectral analysis and the spectral shift measured by the OSA when the temperature of ethanol is changed from 24.4 to 24.5 °C [9].

Figure 10 shows the phase change measured by ultra-fine spectral analysis and the spectral shift measured by the OSA. When the temperature is changed from 24.4 to 24.5 °C, four data points of spectral shift is measured by the OSA, but more data points can be measured by the ultra-fine spectral analysis based on DOFC. This is because the resolution of OSA is limited to $\Delta\lambda$=0.002 nm. Therefore, OSA cannot distinguish the small changes of refractive index and temperature ($\Delta n = 1.4\times10^{-5}$ and $\Delta T = 0.033$ °C). In contrast, ultra-fine spectral analysis based on DOFC can achieve a phase resolution of 0.0017 Rad, which is determined by the minimum frequency spacing of DOFC. Therefore, the ultra-fine spectral analysis can detect smaller changes of refractive index and temperature ($\Delta n = 8.4\times10^{-8}$ and $\Delta T = 2\times10^{-4}$ °C). The sensitivity of the ultra-fine spectral analysis based on DOFC is 167 higher than that of the OSA in terms of refractive index and temperature changes.

Table 1. List of thermo-optic coefficients and their error ranges measured by different methods [9]

	Thermo-optic coefficient of ethanol dn/dT($°C^{-1}$)	Error	Measured conditions
OSA measured	$(-4.9\pm2.2)\times10^{-4}$	45%	24.5 °C, 1550 nm
DOFC method	$(-4.328\pm0.009)\times10^{-4}$	0.2%	24.5 °C, 1550 nm
Fresnel reflection method	$(-4.28\pm0.08)\times10^{-4}$	1.8%	18-56°C, 1550 nm
Fiber Bragg grating [32]	$(-3.99\pm0.2)\times10^{-4}$	5.0%	21.0 °C, 1550 nm

To verify the high resolution and accuracy of ultra-fine spectral analysis based on DOFC, the thermal-optic coefficient (TOC) of ethanol is experimentally measured by different methods. Fig. 11 and Table 1 shows the TOCs and their error ranges measured by different methods. Compared with the value of $(-3.99\pm0.20)\times10^{-4}$ °C^{-1} measured by the fiber Bragg grating refractometer method in the literature [32] and the other value of $(-4.28\pm0.08)\times10^{-4}$ °C^{-1} measured by the Fresnel reflection method, the TOC measured by the ultra-fine spectral analysis based on DOFC is close to the reference data at the temperature ranging from 18 to 56 °C, while the OSA method has a large error range.

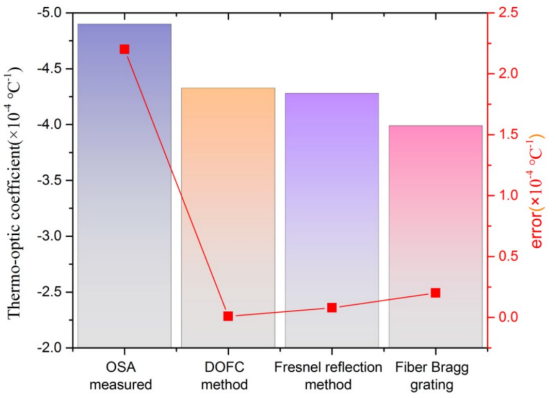

Fig. 11. Thermo-optic coefficients and their error ranges measured by different methods [9].

C. Optical Spectrum Stitching for Ultra-Wide Spectral Analysis

In ultra-fine spectral analysis, the maximum measured frequency range is limited to the bandwidth of the DOFC. For a wider measured frequency range, higher sample rate of DAC is required for generating the DEFC with a wider bandwidth. However, the DAC with high sample rate is expensive, which is not suitable for the cost-sensitive OFS. Here, we demonstrate an optical spectrum stitching (OSS) technique for ultra-fine spectra analysis with a wider measured frequency range [33]. This technique uses tunable laser source (TLS) to move the central wavelength of one DOFC. Then using OSS technique, as shown in Fig. 12, all measured spectra are automatically combined. The interval between two adjacent DOFCs is set to 10 GHz. The ideal optical spectrum of the DUT can be divided into several segments. The bandwidth of each segments is 11 GHz, which has a 1-GHz overlap between adjacent segments. Splice points can also be adjusted to compensate the wavelength shift between two consecutive spectra, which can ensure that the interval of two adjacent spectra before stitching satisfies 10 GHz.

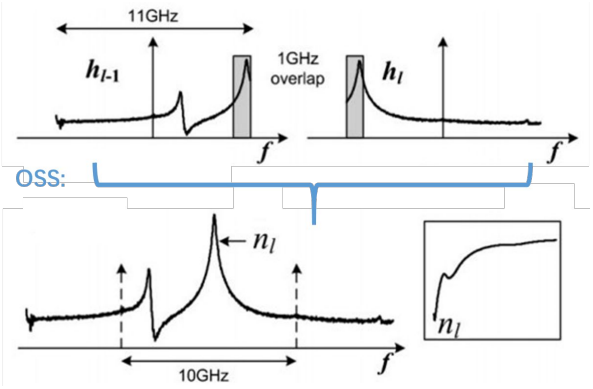

Fig. 12. Principle of the OSS technique [33].

Figure 13 shows the experimental setup for ultra-wide spectral analysis based on ultra-fine spectral analysis and OSS. A stable TLS is used to generate the optical carrier. The generated DEFC is modulated on the optical carrier to generate the DOFC. After DUT, the transmission and reflection optical signals are converted into electrical signal by the digital coherent optical receiver. A real-time oscilloscope is used to convert the recovered DEFC into the digital signal with a sample rate of 25 GS/s. Finally, the ultra-fine spectral analysis and OSS are employed to accurately measure the transmission and reflection spectra of DUT.

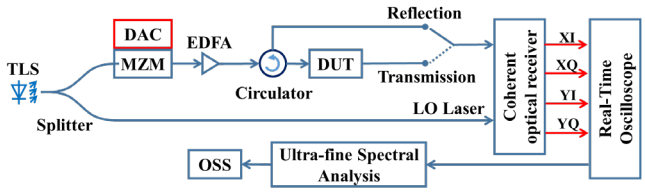

Fig. 13. Experimental setup for ultra-wide spectral analysis based on ultra-fine spectral analysis and OSS [33].

Our experiment employs the FBG-based active FP cavity etched in PM-EDF with 6 mm high- and low-reflection gratings as the DUT to verify the feasibility and advantage of the proposed ultra-wide spectral analysis. Fig. 14 depicts the measured spectra on (a) transmission and (b) reflection paths by OSA (red line) and ultra-wider spectral analysis (blue line). The 2-nm (250-GHz) optical spectra measured by the OSA and ultra-wide spectral analysis almost coincides with each other. The ultra-wide spectral analysis can detect the resonant peak with a frequency width of 310 MHz (2.46 pm), as shown in P4 of Fig. 14 (a). However, the OSAs cannot distinguish this narrow frequency width. However, the ultra-wide spectral analysis can recover the deep optical spectrum notches, as shown in P5 of Fig. 14 (b). In short, the ultra-wider spectral analysis based on OSS and ultra-fine spectral analysis has superior performance in terms of resolution compared with the OSA.

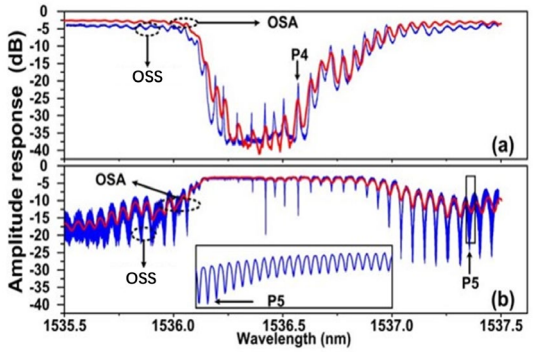

Fig. 14. Measured spectra on (a) transmission and (b) reflection paths by OSA (red line) and ultra-wider spectral analysis (blue line) techniques [33].

IV. BOTDA Based on DOFC for Distributed OFS

BOTDA has gained great attention owing to high spatial resolution for monitoring strain and temperature changes along the fiber under test [34-36]. In conventional BOTDA-based sensing, frequency-sweeping of the probe signal is essential to guarantee sufficient coverage of Brillouin frequency shift (BFS). BFS is subsequently used to monitor the temperature and strain fluctuations.

Typically, the probe or pump signal should be swept more than 100 times around the frequency range of the BFS to capture Brillouin amplification characteristics at different positions along the fiber. The long-time sweep limits the speed for the demodulation of the BFS distribution [37-39]. Hence, it limits the overall sensing speed. The DOFC technology is also proved to be an effective technique for alleviating the restriction of measurement speed [40-42].

In this section, we introduce our progresses on BOTDA based on DOFC for distributed OFS, including BOTDA based on ultra-fine DOFC without scanning, single-shot BOTDA based on phase detection of DOFC, and spatial resolution improvement of single-shot DOFC based BOTDA utilizing multiple pump pulses.

A. Scanning-Free BOTDA Based on DOFC

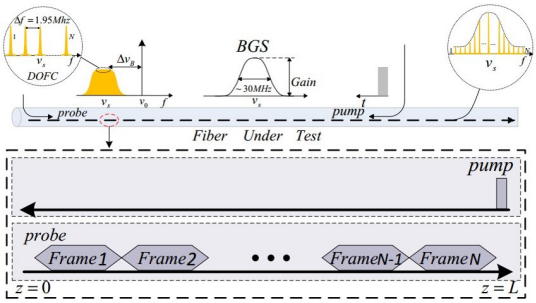

Fig. 15. Principle of scanning-free BOTDA based on DOFC for distributed OFS [39].

Figure 15 depicts the principle of BOTDA based on DOFC for distributed OFS. In conventional BOTDA, a single tone probe is employed. In our proposed scheme, a wide-band DOFC probe is launched into the fiber under test (FUT). Meanwhile, a single-tone pump is injected at the end of FUT. In general, the BFS of the single mode fiber distributes around the frequency of ~11 GHz with a width of 1 GHz. The generated DOFC probe covers the frequency range of the BFS. In the FUT, the DOFC frames interact with single-tone pump successively. Therefore, at the receiver end, the spectrum of DOFC probe is distorted by stimulated Brillouin scattering (SBS). The distributed BFS can be measured by the ultra-fine spectral analysis based on the DOFC. The environmental characteristic such as temperature and strain distributed along the FUT can be acquired from the measured BFS.

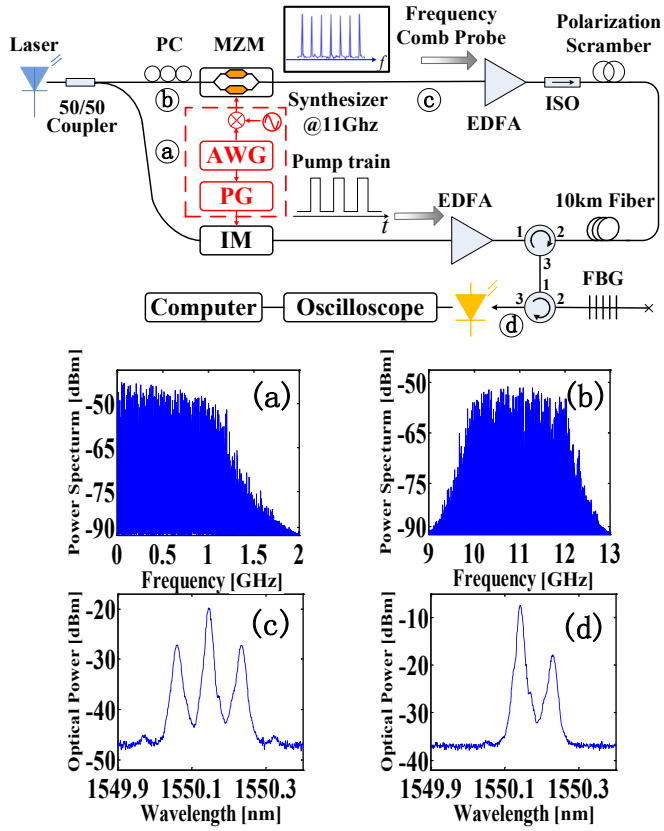

Fig.16. Experimental setup of the scanning-free BOTDA based on DOFC for distributed OFS [39].

Figure 16 depicts the experimental setup of the BOTDA based on DOFC without scanning for distributed OFS. In the experiment, a TLS with a wavelength of 1550 nm and linewidth of 100-kHz is firstly split into two branches: one is for the DOFC probe and the other is for backward pump. For covering the frequency range of BFS, the generated baseband DEFC is mixed with an 11-GHz radio-frequency (RF) signal. Then, a MZM is employed to modulate the optical source with the RF DEFC for generate the RF DOFC. After the EDFA, the launch optical power is set to 0 dBm. The SBS of FUT is induced by the single-tone pump with an average power of 0 dBm, width of 100 ns, repetition frequency of 8.2 kHz, and extinction ratio of ~35 dB. At the receiver, the optical signal is firstly filtered by a narrow-band FBG. A PD converts the filtered optical signal into electrical signal. The recovered signal is fed into the real-time oscilloscope with sample rate of 50 GS/s to generate the digital signal. Finally, the DSP is used to capture the BFS.

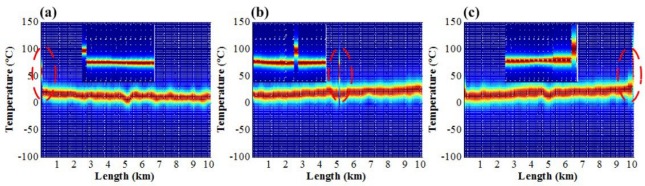

Fig. 17. Measured temperature at the (a) first 51-m fiber, (b) middle 51-m fiber and (c) last 51-m fiber of 10-km FUT [39].

To verify the feasibility of the BOTDA based on DOFC, the temperatures are measured at the first 51-m fiber, middle 51-m fiber and last 51-m fiber of the 10-km FUT, as shown in Fig. 17. The 60 ºC temperature is set at three positions of FUT. To improve the SNR of measured DOFC, 100 acquisitions are required and each acquisition needs 100 μs. Therefore, the total time of one measurement is approximately 10 ms. Under the same setups, the measurement speed of the BOTDA based on DOFC is 2 orders of magnitude faster than the conventional BOTDA at least.

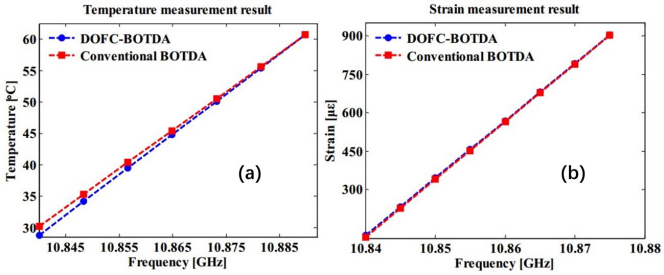

Fig. 18. (a) Estimated temperature and (b) estimated strain against measured BFS by the BOTDA based on DOFC and conventional BOTDA [39].

Figure 18 (a) shows the estimated temperature against measured BFS by BOTDA based on DOFC and conventional BOTDA. For obtaining the temperatures from 30 to 60 ºC with a step of 5 ºC, a thermal chamber is employed to heat the first 51-m fiber of the 10-km FUT. The temperature coefficient of FUT is calculated to be 0.79 ºC/MHz by the BOTDA based on DOFC, which is almost the same with the calculated results by the conventional BOTDA. The maximum deviation of the measured temperature is approximately 0.5 ºC.

Figure 18 (b) depicts the estimated strain against measured BFS by the BOTDA based on DOFC and conventional BOTDA. Firstly, we fix one end of 51-m fiber on the base plate of the optical bench. Meanwhile, a displacement platform is used to stretch the other end to gradually increase the strain from 0 to 900 με with a step of ~110 με. The strain change of 110 με corresponds to a frequency shift of 5 MHz. The strain coefficient of FUT is calculated to be 22.5 με/MHz by the BOTDA based on DOFC, which is almost the same with the calculated results by the conventional BOTDA. The maximum deviation of the measured strain is less than 19 με.

B. Single-Shot BOTDA Based on DOFC and Coherent Detection for Distributed OFS

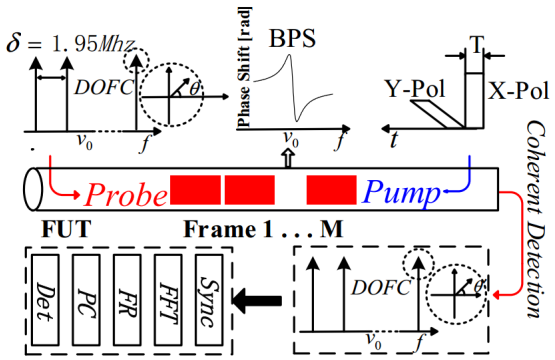

Fig. 19. Principle of single-shot BOTDA based on DOFC and coherent detection for distributed OFS [43].

The above scanning-free BOTDA scheme employs the direct detection. Because of the limited signal–to-noise ratio (SNR) of measured DOFC, many acquisitions are required to improve the measurement accuracy of BOTDA scheme based on direct detection. In the BOTDA based on DOFC and coherent detection, the Brillouin phase shift (BPS) has been proved to be quasi linear near BFS, which is much more sensitive than the intensity change near the Brillouin gain peak. Therefore, BPS is a promising candidate for BOTDA [43]. The high-sensitivity BPS has been used to measure the dynamic strain, which has the advantages of the tolerance to the change of optical fiber attenuation or pump power [44].

Figure 19 shows the principle of single-shot BOTDA based on DOFC and coherent detection for distributed OFS. The DOFC generation in single-shot BOTDA is similar to that in scanning-free BOTDA. However, a predefined phase offset is applied to the input signal of IFFT for generating a DEFC in single-shot BOTDA. The optical modulator is used to modulate the optical source with the DEFC to generate a DOFC with the same initial phase.

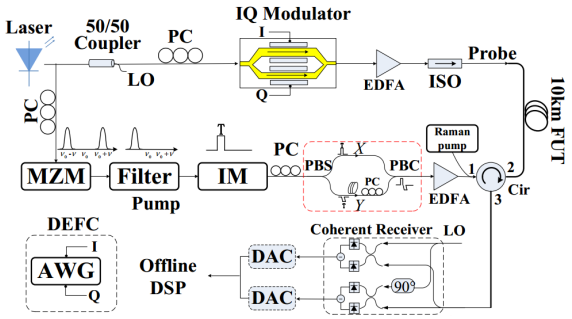

Fig. 20. Experimental setup of the single-shot BOTDA based on DOFC and coherent detection for distributed OFS [43].

Figure 20 shows the experimental setup of the single-shot BOTDA based on DOFC and coherent detection for distributed OFS. The DOFC and pump employ the same laser source. For the DOFC generation, the IQ modulator is employed to modulate the optical source with the DEFC. The generated DOFC has a frequency range of 1 GHz and minimum frequency spacing of 1.95 MHz. After EDFA, the DOFC with optical power of 3 dBm is fed into the FUT. For backward pump generation, the up-conversion operation for the optical source

is implemented by MZM. The carrier rejection by the IQ modulator exceeds 30 dB. Then, the narrow-band optical FBG filter is used to select the high-frequency sideband optical source. An intensity modulator is used to modulate the high-frequency sideband optical source with the pulse sequence with a pulse width of 100 ns and a repetition rate of 8.3 kHz to generate the optical pulse sequence. Then, the generated optical pulse sequence is split into the X-polarization and Y-polarization optical signals by the polarization beam splitter (PBS). Polarization control (PC) is used to adjust the state of polarization (SOP) of the optical signal before PBS to ensure the same power of optical signal on the two polarization paths after PBS. A 20-m SMF is added to the Y-polarization path, which is equivalent to pulse delay of 100 ns. A PC is used to align the polarization state of Y-polarization signal to the polarization beam combiner, which combines the X-polarization and the delayed Y-polarization optical signals to generate the pump. After the EDFA, the average power of pump is set to 0 dBm. At the receiver end, the BPS can be directly obtained by the integrated digital coherent optical receiver. The recovered electrical signal from digital coherent optical receiver is captured by the data acquisition card with sample rate of 2 GS/s to generate the digital signal for obtaining the BFS by the DSP.

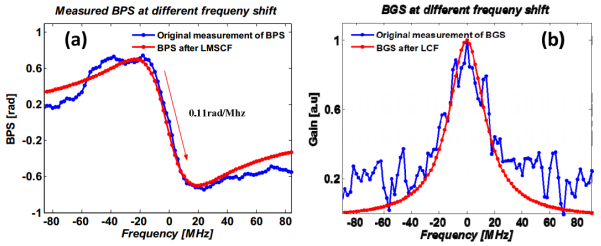

Fig. 21. (a) Brillouin phase spectrum (b) and Brillouin gain spectrum (BGS) measured by the DOFC at the beginning of FUT [43].

The performance of the proposed single-shot BOTDA is verified by using 10-km SMF as the FUT. The FUT has 10.83-GHz BFS distribution at 1550 nm when the room temperature is employed. Fig. 21 (a) shows the measured Brillouin phase spectrum at the beginning of FUT without adding temperature and strain. The linear range of the Brillouin phase spectrum is approximately 40 MHz around the zero frequency. When the least mean square curving fitting is employed, the slope of Brillouin phase spectrum within the linear range is calculated as 0.11 rad/MHz. The BFS can be obtained by finding the center of linear range in the Brillouin phase spectrum. Fig. 21 (b) shows the measured Brillouin gain spectrum (BGS) at the beginning of FUT. The full width at half maximum of BGS is approximately 40 MHz. Therefore, the linear range of the Brillouin phase spectrum is almost the same with the linewidth of the BGS.

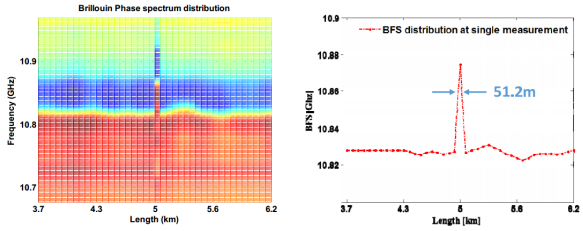

Fig. 22. (a) BPS and (b) BFS measured by the proposed single-shot BOTDA scheme for middle 51-m fiber of FUT when the fiber is heated to 60℃ [43].

To study the spatial resolution of the proposed single-shot BOTDA scheme, we heat the middle 51-m fiber of 10-km FUT. Spatial resolution is determined by the difference of the measured BPS and BFS between the heated and non-heated fiber. Fig. 22 shows the (a) BPS and (b) BFS measured by the proposed single-shot BOTDA scheme for middle 51-m fiber of FUT when the fiber is heated to 60 ℃. The length of a temperature transition is measured as approximately 51.2 m. Therefore, the proposed scheme can reach the spatial resolution of 51.2 m.

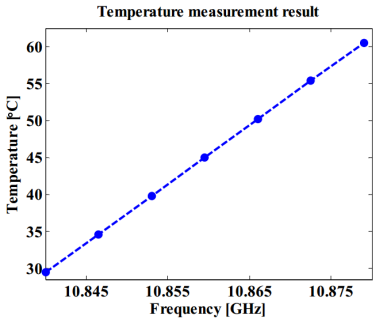

Fig. 23. Linear fitting results of temperature measurement [43].

Figure 23 shows the estimated temperature against measured BPS by single-shot BOTDA. For obtaining the temperatures from 30 ºC to 60 ºC with a step of 5 ºC, a thermal chamber is employed to heat the last 51-m fiber of the 10-km FUT. The maximum deviation of the measured temperature is approximately 0.5 ºC. The temperature coefficient of the fiber was calculated to be 1.25MHz/ºC. We wrapped the fiber of 51 meters over Piezo-ceramic Transducers (PZT) with vibration frequency of 1 kHz for dynamic strain measurement, as shown in Fig. 24 (a). Fig. 24 (b) depicts the measured BFS against time. The sample period is 0.1 ms, corresponding to 10-kHz sampling rate. Therefore, the measurement of BFS has a change rate of 1 kHz, which agrees well with the vibration frequency on the 51 meter fiber. This indicates that the dynamic strain is successfully measured using the proposed scheme.

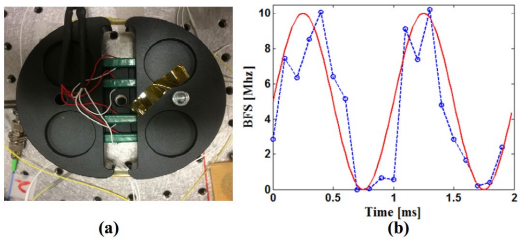

Fig. 24. (a) Piezo-ceramic transducers (PZT) fiber stretcher. (b) Measured BFS against time [43].

C. Spatial Resolution Improvement of Single-Shot DOFC-Based BOTDA Utilizing Multiple Pump Pulses

In DOFC-based BOTDA, the comb spacing of DOFC determines the spectral resolution and the duration of the DOFC frame determines the spatial resolution. There is tradeoff between the high spectral resolution and high spatial resolution. In other words, higher spatial resolution (shorter duration) result in worse detection precision (larger frequency interval) in conventional DOFC-based BOTDA.

Therefore, we propose a single-shot BOTDA scheme based on DOFC to improve the spatial resolution by using multiple pump pulses. As the same with the single-shot BOTDA scheme in Section IV-B, the DOFC probe signal is used to facilitate the acquisition of BGS and BFS without sweeping frequency, resulted in fast BOTDA. Compared with single-pulse pumping, the multi-pump pulses can improve the spatial resolution and maintain the detection accuracy. In the whole demodulation process, the demodulated BGS and BPS do not need any average and maintain the characteristic of single-shot BOTDA.

Figure 25 shows the principle of single-shot DOFC-based BOTDA with four-pump pulse. The DOFC probe is used to measure BGS/BPS. BGS/BPS can be reconstructed to obtain the BFS without frequency scanning. At the end of FUT, four pump pulses with different frequencies are fed into FUT successively at a time interval of 1.2 μs. Therefore, each location of FUT generates four SBS processes with different BFS. The typical BFS of SMF is about 11GHz. To make for BFS in bandwidth of 2 GHz, the frequencies of four pump pulses are set in 11 GHz, 11.402 GHz, 11.804 GHz and 12.206 GHz with the frequency interval of 402 MHz. Among the 402 MHz spacing, 400 MHz is determined by the Brillouin linewidth, the BFS dynamic range and the DOFC frequency interval (multiple of 8MHz) and 2 MHz is used to determine the frequency resolution.

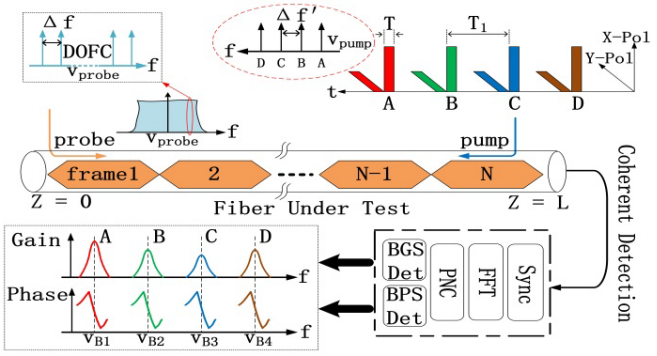

Fig. 25. Principle of single-shot DOFC-based BOTDA with four pumped pulse [45].

The conventional BOTDA based on DOFC has an inverse relationship between detection precision and spatial resolution. Under the action of single pump pulse, considering the spectral resolution and the optimal selection of spatial resolution, we choose the frequency interval precision of 2 MHz on DOFC, which leads to the spatial resolution of 50 m. In the scheme, four pump pulses with a certain frequency interval are replaced by a single pulse signal. The 4 pump pulses interact with the DOFC frame in a certain order in FUT. Each DOFC frame will contain the intensity and phase information of the SBS caused by its covered fiber segment pulse. Therefore, the detection precision does not decrease (2 MHz), and the spatial resolution is increased by four times (12.5 m).

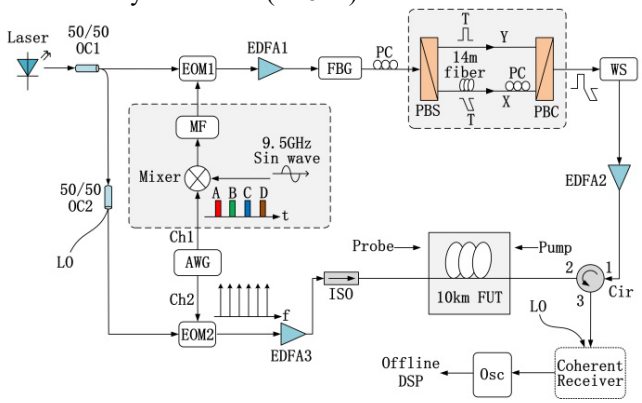

Fig. 26. Experimental setup of the single-shot BOTDA based on DOFC and multiple pump pulses [45].

Figure 26 shows the experimental setup of the single-shot BOTDA based on DOFC and multiple pump pulses. The experimental setup of the single-shot BOTDA based on DOFC and multiple pump pulses is almost similar with that of conventional scheme described above. Four pump pulses are generated by AWG. Then, a RF mixer convert them to the designed frequencies (i.e., 11 GHz, 11.402 GHz, 11.804 GHz and 12.206 GHz). The band-pass microwave filter is used to select out the designed frequencies after the mixer. The pulse width and repetition rate of the pump pulse are 70 ns and 125 μs, respectively.

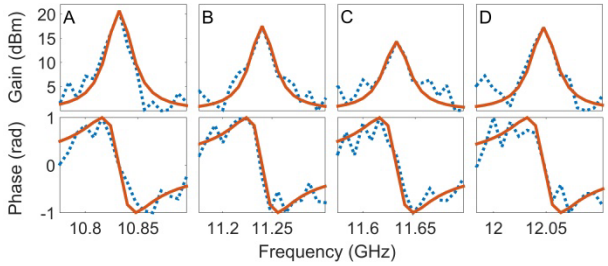

Fig. 27. Four original BGSs and BPSs measured at one position of FUT (red curves are obtained by Lorentzian/linear fitting) [45].

The 10-km FUT in the experiment has a uniform BFS of 10.832GHz. Fig. 27 depicts four original BGSs and BPSs measured at one position of FUT under constant temperature and humidity in the laboratory. As mentioned above, although four BFSs determined by four BGSs are located on the frequency component of DOFC, the peak intensity of each BGS with the frequency difference of 2 MHz is also significantly different, as BGSs in Fig. 27 shows. The peak intensity of four BGS are compared and the BFS of the measured position can be obtained by a simple calculation. The frequency resolution and detection accuracy of our scheme are determined by the frequency difference of 2 MHz, rather than the frequency interval of DOFC. Moreover, the curve of BPS near BFS is quasi linear as depicted in BPSs of Fig. 27, which is more sensitive than the change near the peak intensity of the BGS. Therefore, a higher-precision BFS can be obtained from BPS.

Table 2. Performance chart for DOFC-based BOTDA, existing BOTDA and BOTDR sensors [46]

	DOFC-based BOTDA	Existing BOTDA [39, 47-48]	BOTDR [49]
Measurement Time	100 μs	2-5 min	1-5 min
Spatial resolution	12.5 m @ 10 km	2 m @150 km	1 m @ 20km
Temperature measurement resolution	1.6 ℃	1–2.1 ℃	2-3℃
Strain measurement resolution	44 με	20-45 με	60 με
Sensing Range	10-50 km	150-200 km	20-50 km
Multi-dimensional information (single shot)	Intensity, Phase, Pol.	Intensity	Intensity
Dynamic measurement	yes	yes	No
Detection scheme	Coherent	Direct	Coherent

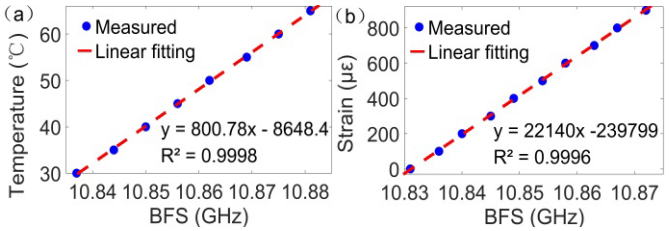

Fig. 28. (a) Measured temperature and (b) measured strain using the proposed single-shot BOTDA [45].

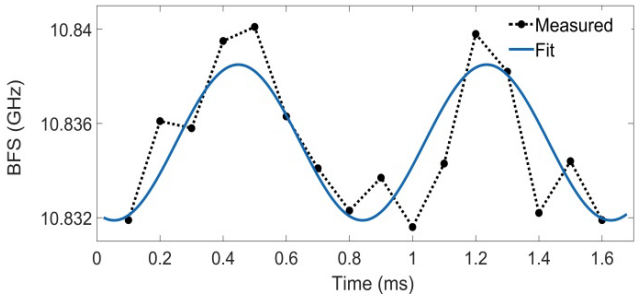

Fig. 29. Measured BFS against time of the fiber with the sinusoidal vibration of the 1.2 kHz based on the PZT [45].

We measure three parameters of the temperature, strain and response speed to verify the performance of the proposed single-shot BOTDA. Figure 28 shows that the optical fiber temperature coefficient of the system is 0.8°C/MHz and the fiber strain coefficient is 22.14 με/MHz. As shown in Fig 29, the sinusoidal vibration of the 1.2 kHz based on the PZT is used to demonstrate that the proposed single-shot BOTDA has high response speed. Finally, two adjacent 12.5-m fiber segments in the middle of FUT are heated to 60°C to verify the spatial resolution of the proposed scheme. Figure 30 depicts that the measured BPSs and BFSs of the heated segments are different from that of the segments at room temperature. The length of the temperature transition is measured as approximately 12.5 m. This experimental result shows that the proposed scheme can reach the spatial resolution of 12.5 m, which is much higher than BOTDA scheme in Section IV-B.

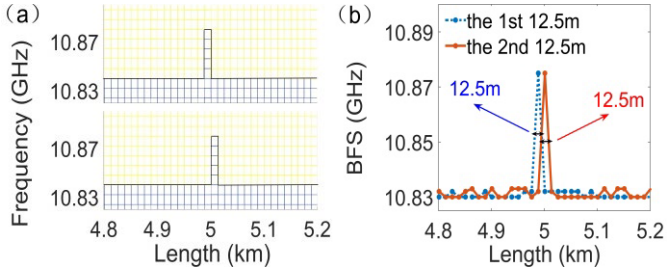

Fig. 30. (a) Measured BPS of the 1st/2nd 12.5m fiber section heated at 60°C and (b) corresponding BFS distribution obtained from (a) [45].

Based on the above discussion, we list the main parameters of our DOFC-based BOTDA and the existing ones, as shown in Table 2.

For the distributed Brillouin sensing, there exist many variations, including the differential pulse-width pair based BOTDA (DPP-BOTDA) [47], frequency scanning BOTDA [39] and BOTDR [49], etc. The DOFC-based BOTDA has the same performance compared to the current technology in terms of the temperature resolution and the stress resolution. Moreover, DOFC-based BOTDA can implement single-shot measurement within 100 μs, which is much faster than the existing BOTDA and BOTDR. Meanwhile, the multi-dimensional measurement can be realized, which provides more dimensions to monitor the physical field distribution along the optical fiber link. However, in terms of spatial resolution, compared to existing BOTDA and BOTDR, DOFC-based BOTDA is worse, which will be the focus of our future research. While maintaining single-shot and ultra-fast measurement unchanged, we hope to further improve the spatial resolution of DOFC-based BOTDA.

V. Conclusion

Fueled by digital coherent optical technologies, optical fiber sensing offers the possibility of multi-dimensional signal processing and information acquisition through digital coherent signal processing. In this paper, we have presented DOFC that digitally generates multiple frequency lines. Combined with digital coherent optical receiver, we have demonstrated multi-

dimensional, high resolution, real-time, time-frequency analysis in the exemplary applications of ultra-fine spectrum analysis and three advanced BOTDA techniques, including scanning-free BOTDA based on DOFC, single-shot BOTDA based on DOFC and coherent detection, and single-shot DOFC-based BOTDA with spatial resolution improvement utilizing multiple pump pulses. We have realized much improved performance and further enhancements will be ensued by extensive implementation of digital coherent optical technologies.

REFERENCES

[1] Z. Chen, G. Hefferman, and T. Wei, "Terahertz-Range Weak Reflection Fiber Optic Structures for Sensing Applications," *IEEE Journal of Selected Topics in Quantum Electronics*, vol. 23, no. 2, Article No. 5600806, 2017.

[2] A. Barrias, J. R. Casas and S. Villalba, "A review of distributed optical fiber sensors for civil engineering applications," *Sensors*, vol. 16, no. 5, Article No. 748, 2016.

[3] B. Lee, "Review of the present status of optical fiber sensors," *Optical Fiber Technology*, vol. 9, no. 2, pp.57-79, 2003.

[4] R. Willsch, W. Ecke, and H. Bartelt, "Optical fiber grating sensor networks and their application in electric power facilities, aerospace and geotechnical engineering," presented at the Optical Fiber Sensors Conference, Portland, OR, USA, May 2002, paper TuA1.

[5] G. Z. Xiao, P. Zhao, F. G. Sun, Z. G. Lu, Zhiyi Zhang, and C. P. Grover, "Interrogating fiber Bragg grating sensors by thermally scanning a demultiplexer based on arrayed waveguide gratings," *Opt. Lett.*, vol. 29, no. 19, pp. 2222-2224, 2004.

[6] H. Guo, G. Xiao, N. Mrad, and J. Yao, "Fiber Optic Sensors for Structural Health Monitoring of Air Platforms," *Sensors*, vol. 11, no. 4, pp. 3687-3705, 2011.

[7] D. Psaltis, "Coherent Optical Information Systems," *Science*, vol. 298, pp. 1359-1363, 2002.

[8] L. Kazovsky, "Multichannel coherent optical communications systems," *Journal of Lightwave Technology*, vol. 5, no. 8, pp. 1095-1102, 1987.

[9] Y. Bao, X. Yi, Z. Li, Q. Chen, J. Li, X. Fan, and X. Zhang, "A digitally generated ultrafine optical frequency comb for spectral measurements with 0.01-pm resolution and 0.7-μs response time," *Light: Science & Applications*, vol. 5, Article No. e300, 2015.

[10] P. Dean, M. R. Dickinson, and D. P. Westa, "Full-field coherence-gated holographic imaging through scattering media using a photorefractive polymer composite device," *Appl. Phys. Lett.*, vol. 85, no. 3, pp. 363-365, 2004.

[11] C. Liu, Z. Dutton, C. H. Behroozi, and L. V. Hau, "Observation of coherent optical information storage in an atomic medium using halted light pulses," *Nature*, vol. 409, pp. 490-493, 2001.

[12] S. Tsukamoto, D.-S. Ly-Gagnon, K. Katoh, and K. Kikuchi, "Coherent demodulation of 40-Gbit/s polarization-multiplexed QPSK signals with 16-GHz spacing after 200-km transmission," presented at the Optical Fiber Communication Conf., Anaheim, CA, USA, Mar. 2005, paper PDP29.

[13] X. Li, X. Chen, G. Goldfarb, E. Mateo, I. Kim, F. Yaman, and G. Li, "Electronic post-compensation of WDM transmission impairments using coherent detection and digital signal processing," *Opt. Express*, vol. 16, no. 2, pp. 880-888, 2008.

[14] S. J. Savory, "Digital filters for coherent optical receivers," *Opt. Express*, vol. 16, no. 2, pp. 804-817, 2008.

[15] G. Li, "Recent advances in coherent optical communication," *Advances in Optics and Photonics*, vol. 1, pp. 279--307, 2009.

[16] M. Salsi, H. Mardoyan, P. Tran, C. Koebele, E. Dutisseuil, G. Charlet, and S. Bigo, "155×100Gbit/s coherent PDM-QPSK transmission over 7,200km," presented at the Eur. Conf. Opt. Commun., Vienna, Austria, Sep. 2009, paper PD2.5.

[17] J. Zhang, J. Yu, B. Zhu, and H. Chien, "WDM Transmission of Single-Carrier 120-GBd ETDM PDM-16QAM Signals Over 1200-km Terrestrial Fiber Links," *Journal of Lightwave Technology*, vol. 35, no. 4, pp. 1033-1040, 2017.

[18] J. Cai, H. G. Batshon, M. V. Mazurczyk, O. V. Sinkin, D. Wang, M. Paskov, W. W. Patterson, C. R. Davidson, P. C. Corbett, G. M. Wolter, T. E. Hammon, M. A. Bolshtyansky, D. G. Foursa, and A. N. Pilipetskii, "70.46 Tb/s Over 7,600 km and 71.65 Tb/s Over 6,970 km Transmission in C+L Band Using Coded Modulation With Hybrid Constellation Shaping and Nonlinearity Compensation," *Journal of Lightwave Technology*, vol. 36, no. 1, pp. 114-121, 2018.

[19] X. Yan, X. Zou, W. Pan, L. Yan, and J. Azaña, "Fully digital programmable optical frequency comb generation and application," *Opt. Lett.*, vol. 43, no. 2, pp. 283-286, 2018.

[20] X. Jia, H. Chang, K. Lin, C. Xu, and J. Wu, "Frequency-comb-based BOTDA sensors for high-spatial-resolution/long-distance sensing," *Opt. Express*, vol. 25, no. 6, pp. 6997-7007, 2017.

[21] J. Fang, P. Xu, Y. Dong, and W. Shieh, "Single-shot distributed Brillouin optical time domain analyzer," *Opt. Express*, vol. 25, no. 13, pp. 15188-15198, 2017.

[22] S. Pan and M. Xue, "Ultrahigh-Resolution Optical Vector Analysis Based on Optical Single-Sideband Modulation," *J. Lightwave Technol.*, vol. 35, no. 4, pp. 836-845, 2017.

[23] Y. Han and G. Li, "Coherent optical communication using polarization multiple-input-multiple-output," *Opt. Express*, vol. 13, no. 19, pp. 7527-7534, 2005.

[24] W. Shieh and C. Athaudage, "Coherent optical orthogonal frequency division multiplexing," *Electron. Lett.*, vol. 42, no. 10, pp. 587-589, 2006.

[25] W. Shieh, H. Bao, and Y. Tang, "Coherent optical OFDM: theory and design," *Opt. Express*, vol. 16, no. 2, pp. 841-859, 2008.

[26] W. Shieh, X. Yi, Y. Ma, and Q. Yang, "Coherent optical OFDM: has its time come? [Invited]," *J. Opt. Netw.* vol. 7, no. 3, pp. 234-255, 2008.

[27] S. J. Savory, "Digital Coherent Optical Receivers: Algorithms and Subsystems," *IEEE Journal of Selected Topics in Quantum Electronics*, vol. 16, no. 5, pp. 1164-1179, 2010.

[28] S. L. Jansen, I. Morita, T. C. Schenk, and H. Tanaka, "Long-haul transmission of16×52.5 Gbits/s polarization-division- multiplexed OFDM enabled by MIMO processing (Invited)," *J. Opt. Netw.* vol. 7, no. 2, pp. 173-182, 2008

[29] X. Yi, W. Shieh, and Y. Tang, "Phase Estimation for Coherent Optical OFDM," *IEEE Photon. Tech. Lett.*, vol. 19, no. 12, pp. 919-921, 2007.

[30] X. Yi, W. Shieh, and Y. Ma, "Phase Noise Effects on High Spectral Efficiency Coherent Optical OFDM Transmission," *J. Lightwave Technol.*, vol. 26, no. 10, pp. 1309-1316, 2008.

[31] X. Yi, Z. Li, Y. Bao, and K. Qiu. "Characterization of passive optical components by dsp-based optical channel estimation," *IEEE Photonics Technology Letters*, vol. 24, no. 6, pp. 443-445, 2012.

[32] R. C. Kamikawachi, I. Abe, A. S. Paterno, H. J. Kalinowski, M. Muller, J. L. Pinto, J. L. Fabris, "Determination of thermo-optic coefficient in liquids with fiber Bragg grating refractometer," *Opt. Comm.*, vol. 281, no. 4, pp. 621-625, 2008.

[33] C. Jin, Y. Bao, Z. Li, T. Gui, H. Shang, X. Feng, J. Li, X. Yi, C. Yu, G. Li, and C. Lu, "High-resolution optical spectrum characterization using optical channel estimation and spectrum stitching technique," *Opt. Lett.*, vol. 38, no. 13, pp. 2314-2316, 2013.

[34] T. Horiguchi and M. Tateda, "BOTDA-nondestructive measurement of single-mode optical fiber attenuation characteristics using Brillouin interaction: theory," *Journal of Lightwave Technology*, vol. 7, no. 8, pp. 1170-1176, Aug 1989.

[35] Y. Peled, A. Motil, and M. Tur, "Fast Brillouin optical time domain analysis for dynamic sensing," *Opt. Express*, vol. 20, no. 8, pp. 8584-8591, 2012.

[36] W. Li, X. Bao, Y. Li, and L. Chen, "Differential pulse-width pair BOTDA for high spatial resolution sensing," *Opt. Express*, vol. 16, no. 26, pp. 21616-21625, 2008.

[37] X. Bao and L. Chen, "Recent progress in optical fiber sensors based on Brillouin scattering at university of Ottawa," *Photon. Sensors*, vol. 1, no. 2, pp. 102–117, 2011.

[38] T. Sperber, A. Eyal, M. Tur, and L. Thévenaz, "High spatial resolution distributed sensing in optical fibers by Brillouin gain-profile tracing," *Opt. Express*, vol. 18, no. 8, pp. 8671–8679, 2010.

[39] M. A. Soto, G. Bolognini, and F. Di Pasquale, "Optimization of long-range BOTDA sensors with high resolution using first-order bi-directional Raman amplification," *Opt. Express*, vol. **19,** no. 5, pp. 4444-4457, 2011.

[40] C. Jin, N. Guo, Y. Feng, L. Wang, H. Liang, J. Li, Z. Li, C. Yu, and C. Lu, "Scanning-free BOTDA based on ultra-fine digital optical frequency comb," *Opt. Express*, vol. 23, no. 4, pp. 5277--5284, 2015.

[41] C. Zhao, M. Tang, L. Wang, H. Wu, Z. Zhao, Y. Dang, J. Wu, S. Fu, D. Liu, P. Shum, "BOTDA using channel estimation with direct-detection

optical OFDM technique," *Opt. Express*, vol. 25, no. 11, pp. 12698--12709, 2017.
[42] J. Fang, P. Xu, and W. Shieh, "Single-shot measurement of stimulated Brillouin spectrum by using OFDM probe and coherent detection," presented at the Australian Conference on Optical Fibre Technology, Sydney, Australia, Sept. 2016, paper AT5C.3.
[43] C. Jin, L. Wang, Y. Chen, N. Guo, W. Cheung, H. Au, Z. Li, H. Tam, and C. Lu, "Single-measurement digital optical frequency comb based phase-detection Brillouin optical time domain," *Opt. Express*, vol. 25, no. 8, pp. 9213-9224, 2017.
[44] J. Urricelqui, A. Zornoza, M. Sagues, and A. Loayssa, "Dynamic BOTDA measurements based on Brillouin phase-shift and RF demodulation," *Opt. Express*, vol. 20, no. 24, pp. 26942-26949, 2012.
[45] Z. Liang, J. Pan, S. Gao, Q. Sui, F. Li, Y. Feng, W. Liu and Z. Li, "Spatial resolution improvement of single-shot DOFC based BOTDA utilizing multiple pump pulses," *Opt. Lett to be accepted.*
[46] X. Bao, L. Chen, "Recent progress in distributed fiber optic sensors," *Sensors*, vol. 12, no. 7, pp. 8601, 2012.
[47] W. Li, X. Bao, Y. Li, and L. Chen, "Differential pulse-width pair BOTDA for high spatial resolution sensing," *Opt. Express*, vol. 16, no. 26, pp. 21616-21625, 2008.
[48] Y. Dong, L. Chen, X. Bao, "Extending the Sensing Range of Brillouin Optical Time-Domain Analysis Combining, Frequency-Division Multiplexing and In-Line EDFAs," *Journal of Lightwave Technology*, vol. 30, no. 8, pp. 1161-1167, 2012.
[49] K. Shimizu, T. Horiguchi, Y. Koyamada, and T. Kurashima, "Coherent self-heterodyne detection of spontaneously Brillouin-scattered light waves in a single-mode fiber," *Opt. Letters*, vol. 18, no. 3, pp. 185, 1993.

Jingshun Pan received the B.Sc. and the M.Sc. degrees from South China Normal University, Guangdong, China, in 2009 and 2012, respectively. He is currently a Ph.D. student at Sun Yat-sen University, China. His research interests include optical fiber sensors, optical signal processing technology and ultra-fine measurement systems.

Ji Zhou received the B.E. degree and the Ph.D. degree (with highest honor) in School of Information and Communication Engineering from Beijing University of Posts and Telecommunications, Beijing, China, in 2012 and 2018, respectively. From 2016 to 2017, he was a visiting scholar in the Lightwave Research Laboratory, Department of Electrical Engineering, Columbia University. Since 2018, he is a lecturer in Department of Electrical Engineering, Jinan University. He has authored more than 40 IEEE/OSA journal and conference papers. His research interests include modulation and digital signal processing for optical-wireless communications and optical-fiber communications. He serves as a reviewer of the IEEE/OSA publications and a TPC Member for IEEE conferences, including JLT, OE, PTL, PJ, TCOM, IEEE Access, OECC, and VTC. He received an Outstanding Ph.D. Graduate Award of Beijing, Excellent Doctoral Dissertation Award of Beijing University of Posts and Telecommunications, four National Ph. D. Scholarship of China, two BUPT Excellent Ph. D. Student Foundation, and two Postgraduate Innovation Fund of SICE, BUPT.

Xingwen Yi received the B.Eng. degree in electronic engineering from the Southeast University, Jiangsu, China, in 1999 and the Ph.D. degree in electrical and electronic engineering from the University of Melbourne, Parkville VIC, Australia, in 2007.

From 1999 to 2004, he was with Huawei Technologies, Corporation, Ltd., China. During 2005, he was an Intern for three months at Alcatel SEL AG, Germany. From 2008 to 2009, he was a Research Scientist with the Department of Electrical and Computer Engineering, University of California, Davis, CA, USA. From 2009 to 2018, he joined the School of Communication and Information Engineering, University of Electronic Science and Technology of China, Chengdu, China. Since March 2018, he has been a Professor with the School of Electronics and Information Technology, Sun Yat-sen University, China. He is the author or coauthor of more than 60 journal and conference papers. He holds nine patents in China. His current research interests include optical packet switching, electronic compensation of optical distortions, and optical performance monitoring.

Dr. Yi is a Senior Member of IEEE and Member of the Optical Society of America.

Chao Lu received his B.Eng. degree in electronic engineering from Tsinghua University, Beijing, China, in 1985, and the M.Sc. and Ph.D. degrees from the University of Manchester, Manchester, U.K., in 1987 and 1990, respectively. In 1991, he joined the School of Electrical and Electronic Engineering, Nanyang Technological University, Singapore as a faculty member and was there until 2006. From June 2002 to December 2005, he was seconded to the Institute for Infocomm Research, Agency for Science, Technology and Research, Singapore, as a Program Director and Department Manager, helping to establish a research group in the area of optical communication and fiber devices. Since April 2006, he has been a Professor with the Department of Electronic and Information Engineering, The Hong Kong Polytechnic University, Hong Kong. His research interests include optical communication systems and networks, fiber devices for optical communication, and sensor systems. He is a fellow of OSA.

Zhaohui Li obtained his BS in the department of Physics and MSc in the institute of modern optics from Nankai University, China in 1999 and 2002 respectively, and his PhD from the Nanyang Technological University 2007. Now, he is working in the school of Electronics and Information Technology, Sun Yat-sen University, China as professor in 2009.His research interests are optical communication systems, optical signal processing technology and ultra-fine measurement systems.